



## In Vitro Behavior of Mechanically Activated Nanosized Si-Mg-Doped Fluorapatite

T. Ahmadi<sup>a\*</sup>, A. Monshi<sup>a</sup>, V. Mortazavi<sup>b</sup>, M.H. Fathi<sup>a,b</sup>, B. Hashemibeni<sup>c</sup>, A. Sharifnabi<sup>a,d</sup>

<sup>a</sup>Department of Materials Engineering, Isfahan University of Technology, Isfahan, Iran

<sup>b</sup>Department of Operative Dentistry, Isfahan University of Medical Sciences, Isfahan, Iran

<sup>c</sup>Department of Anatomical Sciences and Molecular Biology, Isfahan University of Medical Sciences, Iran

<sup>d</sup>Department of Metallurgy and Materials Engineering, Iran University of Science and Technology, Tehran, Iran

### PAPER INFO

#### Paper history:

Received 19 September 2015

Accepted in revised form 20 October 2015

#### Keywords:

Mechanical Activation  
Si-Mg-Doped Fluorapatite  
Nanostructured Materials  
In-Vitro Cytotoxicity  
In-Vitro Bioactivity  
Biomedical Applications

### ABSTRACT

Hydroxyapatite (HA) is perhaps the most attractive material for bone repair, replacement and regeneration due to its chemical composition and crystallographic structure which are similar to those of natural bone mineral. However, replacement of various elements and compounds in HA could improve biological properties of this material. Aim of this study was in vitro bioactivity and cellular behavior evaluation of mechanically activated nanosized Silicon and Magnesium co-doped Fluorapatite (Si-Mg-FA). In vitro bioactivity was evaluated in simulated body fluid (SBF) at 37°C for up to 28 days. The apatite precipitates were proved with Scanning Electron Microscopy (SEM) and Fourier Transformed Infrared Spectroscopy (FTIR). Cell viability and cell attachment were studied by MTT assay and scanning electron microscopy (SEM). In vitro examinations revealed the amount of bone-like apatite precipitated on Si-Mg-FA nanopowder was significantly higher than FA. The cell culture medium containing Si-Mg-FA showed more cell proliferation and cell viability than FA. It could be concluded that doping Si and Mg into FA improves the bioactivity and cell viability, therefore, Si-Mg-FA has a good potential to be used as bone substitution material.

## 1. INTRODUCTION

Many types of bioceramics such as hydroxyapatite, bioactive glasses, bioactive silicate-based ceramics and etc., have been presented for bone substitution, bone tissue engineering and as the coating for metal implants so as to accelerate osteo integration [1]. Among these bioceramics, hydroxyapatite [ $\text{Ca}_{10}(\text{PO}_4)_6(\text{OH})_2$ , HA] is of great importance because of its similarity to mineral part of bone in respect to chemical composition and crystallographic structure [2]. The apatite properties depend on its crystallinity, chemistry, density, secondary phases and also environmental conditions such as pH [3]. Bone mineral contains several ionic substitutions in comparison to synthesized HA [4]. There are several trace compounds and elements such as  $\text{CO}_3^{2-}$ ,  $\text{Na}^+$ ,  $\text{K}^+$ ,  $\text{Mg}^{2+}$ ,  $\text{Cl}^-$ ,  $\text{SiO}_4^{4-}$  and  $\text{F}^-$  in the structure of biological apatite [5, 6]. Magnesium, which is the fourth most abundant element in the living bodies, is essential for bone mineralization, mechanical properties and also for cellular and enzymatic reactions [7,8]. Calcium can be partially substituted by Magnesium.

Presence of fluorine in saliva and blood plasma is important for normal skeletal and dental development [9]. Fluoride ions replace hydroxyl groups in the apatite lattice structure, leading to the formation of fluorapatite (FA). Fluoride ions yields higher stability for apatite and thereby decrease the solubility of FA in comparison to HA [10]. Fluorine ions suppress dental and bone caries [11]. Moreover, FA not only provides greater protein adsorption and cell attachment with respect to HA [12], but also promotes proliferation, morphology and differentiation of osteoblast cells [13]. Silicon plays a critical role in the bone calcification process. Doping the silicate groups into HA enhances its osteoblast cell activity [14]. Silicon-substituted apatites have been prepared by different methods including sol-gel, hydrothermal, solid state reaction, controlled crystallization, and etc. [15]. According to Hench's researches, loss of biological silicon deteriorates the proliferation and function of osteoblasts causing the subsequent osteopenia and osteoporosis. Bone cells proliferate more rapidly in the presence of soluble Silicon [16].

Therefore, in this research F, Mg and Si were incorporated into the HA structure to stimulate the formation of biological apatite. Mechanical activation

\*Corresponding Author's Email: [tahmadi56@yahoo.com](mailto:tahmadi56@yahoo.com) (T. Ahmadi)

by high energy ball milling was selected to fabricate FA nanoparticles, silicon and magnesium co-doped fluorapatite (Si-Mg-FA). Mechanical activation is a simple solid-state method for preparing nanosized powders [17]. Parameters such as rotation speed, clash frequency, ball-to-powder weight ratio, milling atmosphere, time and temperature as well as the purity, size and shape of powder particles affect the mechanical activation of products [18]. Recently, pure Si-Mg-FA ceramic with approximate crystallite size of 40 nm was synthesized by our group using 12h mechanical activation method [19]. This study is aimed at investigating the in-vitro bioactivity and cytotoxicity evaluation of Si-Mg-FA nanopowder. This is a potential material as a second phase in polymer matrix composites for bone regeneration applications, e.g. for repairing the alveolar bone of periodontal tissue in periodontal membranes or as a coating material for metal implants.

## 2. MATERIALS AND METHODS

### 2.1. Preparation and characterization of Si-Mg-FA

The Si-Mg-FA nanopowder was prepared by the same process previously reported by the authors [19]. Briefly, a high energy planetary ball mill (Fretch Pulverisette 5) with a 125 ml zirconia vial and four 20 mm diameter zirconia balls at ambient temperature was used to mix and mechano-chemically activate the mixture of phosphorous pentoxide ( $P_2O_5$ , Merck), calcium hydroxide ( $Ca(OH)_2$ , Merck), magnesium hydroxide ( $Mg(OH)_2$ , Merck), calcium fluoride ( $CaF_2$ , Merck) and silicon oxide ( $SiO_2$ , Sigma-Aldrich) powders. The mechano-chemical activation process was performed using ball/powder weight ratio of 25:1 and rotation speed of 250 rpm. Ball milling was executed for 12 hours. The designated degree of  $Ca^{2+}$  substitution by  $Mg^{2+}$  and  $PO_4^{3-}$  by  $SiO_4^{4-}$  in the mixture, was indicated by the x and y value in the general formula of FA ( $Ca_{10-x}Mg_x(PO_4)_{6-y}(SiO_4)_yF_{1.5}$ ), where x and y equal to 0.5. The obtained powder with Si and Mg substitution was denoted as Si-Mg-FA.

X-ray Diffraction (XRD, Philips X'Pert-MPD) with Cu  $K\alpha$  radiation ( $\lambda=0.15418nm$ ) was employed to analyze the phase structure of prepared FA and Si-Mg-FA samples. The experimental X-ray diffraction patterns were compared with the Standards patterns compiled by the Joint Committee on Powder Diffraction and Standards (JCDPS).

The morphology and particle size of the Si-Mg-FA powders were studied and determined using Transmission Electron Microscopy (TEM, Philips CM120) technique. The average particle size was determined considering over 100 particles from the TEM images and using image-analysis software (Image J 1.40g).

### 2.2. Immersion test in simulated body fluid (SBF)

The bioactivity behavior of FA and Si-Mg-FA nanopowders was assessed using a simulated body fluid (SBF) prepared according to Kokubo's procedure [20]. The concentration of ions existing in SBF, listed in Table 1, are similar to that of human body plasma. The obtained powders were subjected to hydraulic pressure (at room temperature) to produce disks with dimension of 12mm (diameter) and mass of ~0.5 g. The disks of FA and Si-Mg-FA were placed inside sterilized bottles and immersed in the SBF for various predicted periods of times up to 28 days at  $37\pm 0.5^\circ C$  in a water bath (NUVENB9). The surface area ( $mm^2$ ) ratio of each sample to SBF solution volume (mL) was fixed at 10 to 1 [20]. The pH of SBF solution was measured at the designated time intervals of immersion using a calibrated pH meter (Crison GLP 21).

**TABLE 1.** SBF ions concentrations in comparison with human blood plasma.

Ion	Ion concentration (mM)	
	Blood plasma	SBF
Na <sup>+</sup>	142	142
K <sup>+</sup>	5	5
Mg <sup>2+</sup>	1.5	1.5
Ca <sup>2+</sup>	2.5	2.5
Cl <sup>-</sup>	103	147.8
HCO <sub>3</sub> <sup>-</sup>	27	4.2
HPO <sub>4</sub> <sup>2-</sup>	1	1
SO <sub>4</sub> <sup>2-</sup>	0.5	0.5
pH	7.2 – 7.4	7.4

In order to study and evaluate the bone-like apatite of synthesized nanopowders as an indication of bioactivity, the FA and Si-Mg-FA disks were placed in sterilized bottles containing SBF solution with a liquid/surface area ratio of 10 mL/cm<sup>2</sup>. The samples were soaked in the SBF at  $37\pm 0.5^\circ C$  for various predicted periods of times of 1, 3, 7, 14, 21 and 28 days, after which they were washed with distilled water and dried at room temperature. Scanning electron microscopy (SEM, Philips XL30) was used to study the morphological changes and subsequent growth of the bone-like HA after immersion in the SBF. In addition, the functional groups of precipitates were analyzed by FTIR spectroscopy to confirm the formation of HA on the surface of samples.

### 2.3. Cell cultures

Human Gingival fibroblast (HGF, NCBI: C-131) were used for cell viability and cell proliferation tests. Cells were obtained from the Pasteur Institute of Iran (Tehran). Fibroblast cells were cultured in Roswell Park Memorial Institute (RPMI, Gibco) medium supplemented with 10% fetal bovine serum and 1% penicillin/streptomycin at  $37^\circ C$  and in humidified atmosphere containing 5% CO<sub>2</sub>. The cell morphology at culture medium was observed by an inverted microscope (Nikon, TEU 2000). When the cells were confluence, they were trypsinized (0.25%

trypsin/0.2% EDTA; Sigma), and  $5 \times 10^4$  of them were counted and placed into each well of a 12-well micro plate. After 24 h, the medium was changed to one containing ionic products from the dissolution of FA and Si-Mg-FA nanopowders. For preparation of this solution, 2 g of FA and Si-Mg-FA were dissolved in 20 ml medium (RPMI +10% FBS+1% Penicillin/Streptomycin). After 48 h, this solution was sterilized with a 0.2  $\mu\text{m}$  filter. The culture without extracts was used as the control sample. Extracts for indirect tests were obtained from the materials under standardized conditions (ISO 10993-5). The MTT [3-(4, 5-dimethylthiazol-2-yl)-2, 5-diphenyl tetrazolium Bromide, Sigma] solution was used in order to measure the cell viability and proliferation. After culture of the cells for 24, 72 and 168 h, the supernatant was removed from each well and the cells were rinsed with phosphate-buffered saline (Sigma) to eliminate nonviable cells. 800  $\mu\text{l}$  serums - free medium and 80  $\mu\text{l}$  MTT solution was added to each well and the cells were incubated at 37°C for 4 h to allow the formation of formazan crystals. After incubation, the supernatant was removed, and 400  $\mu\text{l}$  dimethyl sulfoxide (Sigma) was added to dissolve the formazan crystals. Then 100  $\mu\text{l}$  of the solution was transferred to a 96-well plate and absorbance of each well was determined by an ELISA reader (Hiperion MPR4) at 570 nm. The cell viability percentage was calculated using the below equation (OD means optical density):

$$\text{cell viability}\% = (\text{OD of sample}) / (\text{OD of control}) \times 100 \quad (1)$$

#### 2.4. Statistics

One way analysis of variance (ANOVA) with the Tukey's post hoc test was used to compare the MTT results. P-values < 0.05 was taken to be significant.

#### 2.5. Cell attachment

Cell attachment evaluations were performed by SEM images scanning electron microscopy (SEM, Philips XL30). For this purpose,  $10^4$  cells were cultured on the disks of FA and Si-Mg-FA and placed in the wells of a 12-wells plate for 24 h and 72 h. Then cells on the samples were rinsed three times with phosphate buffer solution (PBS, pH 7.4). They were fixed by 2.5% glutaraldehyde solution. The samples were dehydrated in 30, 50, 70, 90, 95 and 100vol% alcohol solutions. Finally, the samples were coated with Gold and attached cells were studied and observed by SEM.

### 3. RESULT AND DISCUSSION

#### 3.1. Characterization of Si-Mg-FA nanopowder

Characterization of the obtained nanopowders has been discussed in detail in the author's former paper [19]. Figure 1(a) shows the XRD patterns of Si-Mg-FA powder after 12h ball-milling. The XRD peaks related to FA (standard card #15-0876) appears after 12 h

milling. According to TEM image (Figure 1(b)), the Si-Mg-FA nanoparticles with agglomerated spherical morphology and particle size of < 100 nm are clearly observed. The mean particle size is  $31.184 \pm 7.452$  nm [19].

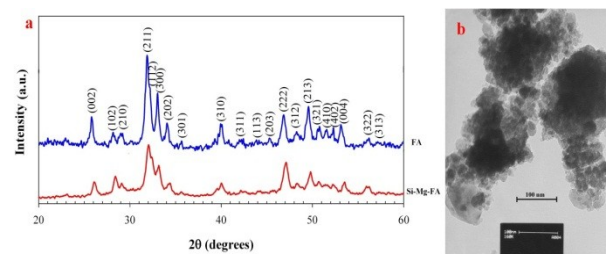


**Figure 1.** a) XRD patterns of Si-Mg-FA and FA, and b) TEM image of Si-Mg-FA apatite nanopowder [19].

#### 3.2. In vitro bioactivity

In vitro bioactivity behavior of Si-Mg-FA and FA nanopowders was examined in the SBF under physiological condition (pH of 7.4 at 37°C) for a predetermined time intervals up to 4 weeks. This method is known to be both qualitative and quantitative. SBF immersion test is used to screen the bone bioactive materials before animal testing. Thus, the number of animals tested and the duration of animal experiments can be remarkably reduced by using this method. It is well-established that the biomaterial bonds to the newly formed bone through the carbonated HA layer precipitated at the biomaterial/bone interface. Therefore, this supervision helps to estimate not only in vivo bone bioactivity but also in vivo implant-bone interfacial reactions [20]. SBF contains inorganic ions with concentrations similar to human plasma and it does not contain any factors involved in osteogenesis, such as proteins or specific trace elements [21]. Figure 2. shows the pH values of SBF versus immersion days. As for SBF without any immersed sample, the pH value remained nearly constant around 7.4.

The FA has low dissolution in SBF and apatite nucleates from the first immersion day; therefore, the pH of SBF is decreased. Similar results can be observed for Ca, P, Mg ions concentrations in SBF after soaking the samples in SBF [19]; that is, concentrations of these elements are decreased after soaking FA samples due to low solubility of FA in SBF which causes the immediate apatite nucleation, and also is in agreement with pH variations.

According to Figure 2. pH of SBF in which the Si-Mg-FA samples are immersed, is increased in the first three days of soaking and then is decreased. Si-Mg-FA has faster dissolution rate than FA because substitution of Si and Mg in FA structure decreases the crystallinity and crystallite size of the nanoparticles resulting in the higher dissolution rates [19]. The pH variations are in accordance with the Ca, P, Si and Mg concentrations [19]. The Ca, P and Mg concentrations in SBF is increased during the first three days, signifying that

dissolution overcomes the nucleation over this period. After 3 days, formation of thermodynamically stable apatite crystals from supersaturated SBF takes place [22].

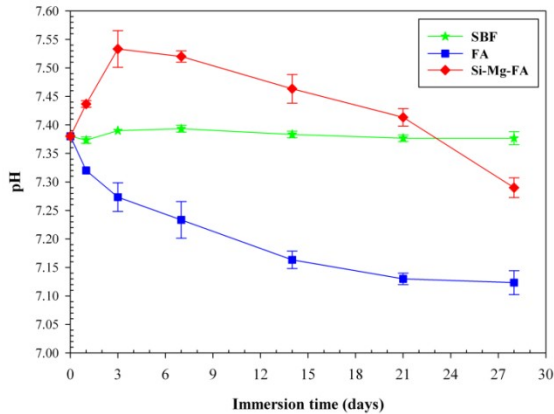


**Figure 2.** pH values of SBF solution versus incubation time at  $37\pm 0.5^\circ\text{C}$  for FA and Si-Mg-FA samples.

The bone-like apatite precipitation on the surface of samples is verified by SEM. Figure 3. demonstrates the formation and growth of apatite crystals on the surface of the powders after being soaked in the SBF solutions for various times. The apatites precipitated on the surfaces of each sample are mostly agglomerated. Furthermore, the average size and the number of agglomerated precipitates on the surface of each sample are increased as a result of increasing the incubation time. Moreover, in comparison with the FA sample, both quantity and size of precipitates formed on the surface of Si-Mg-FA sample are higher at different soaking times. The process and kinetics of apatite formation on HA surface can be affected by bulk factors including density and surface area, and also by surface factors such as composition and structure [23]. Normal SBF does not provide sufficient supersaturation for Ca and P ions required for spontaneous nucleation while it is sufficient for the apatite crystal growth. Thus, higher supersaturation of Ca and P in the SBF near the solid surface is required for nucleation rather than for crystal growth. The apatite nucleation occurs only if the local Ca ion concentration in SBF near the surface of samples reaches a certain level higher than that of SBF standard [24]. Furthermore, the nucleation rate is exponentially increased with supersaturation. Therefore, increasing the concentration of  $\text{Ca}^{2+}$  and  $\text{PO}_4^{3-}$  ions raises the local supersaturation which is beneficial to nucleation and growth of the new apatite crystals [25]. In addition, the higher the level of dissolution, the larger the number of nucleation sites is achieved. As a result, a higher precipitation rate is obtained for the samples with greater dissolution [26]. Si-Mg-FA nanopowders present higher dissolution rate in comparison to FA [19]. Thus, increasing the Ca, P, Mg and Si

concentrations causes the greater local supersaturation, leading to the nucleation and growth of new apatite.

The ion concentration variations in SBF together with the SEM observations of the samples soaked in SBF prove the larger extent of bone-like apatite precipitation on the Si-Mg-FA as compared to FA. In other words, incorporating Mg and Si improves the bioactivity of FA.

**Figure 3.** Proximity of mixtures activated for different times and sintered at  $1390^\circ\text{C}$  in microwave (MWS) and Conventional furnace (CS). □□□

Microwave radiation reduces the diffusion barrier of ions and accelerates diffusion of grain boundary and densification rate [18, 19].

XRD patterns of the samples milled at different times and sintered at  $1390^\circ\text{C}$  (Figure 4.) confirm that cordierite (File 01-085-1722) was the only crystalline phase in all the sintered specimens. Crystallization behavior of cordierite was investigated in the previous work [21].

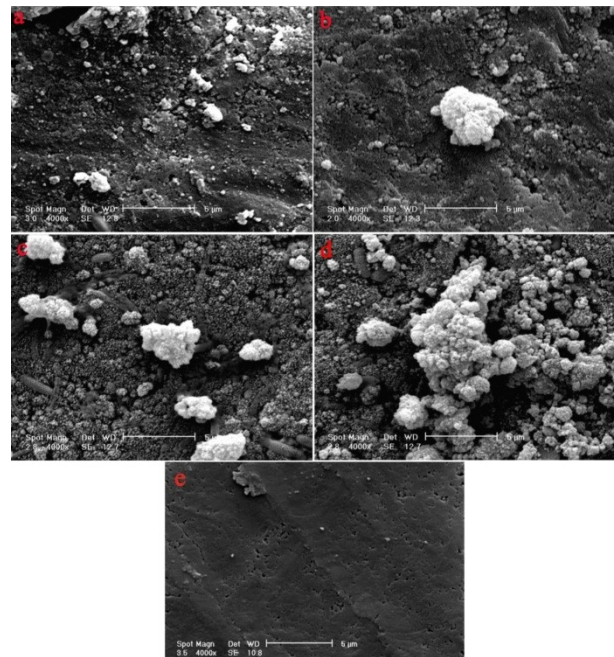


**Figure 3.** SEM images showing the morphology and amount of bone-like apatite formed on the surface of the FA sample after (a) 7 days and (b) 14 days, Si-Mg-FA sample after (c) 7 days and (d) 14 days immersed in SBF at  $37\pm 0.5^\circ\text{C}$  and (e) disk of Si-Mg-FA which is not immersed in SBF.

FTIR spectroscopy was performed on Si-Mg-FA nanopowders before and after being soaked in SBF to study the carbonate hydroxyapatite (CHA) layer formation on the surface. (Figure 4.) Substitution of phosphate groups with carbonate in CHA ( $\text{Ca}_{10}(\text{PO}_4)_{6-x}(\text{CO}_3)_x(\text{OH})_2$ ) clearly decreased the intensities of phosphate bonds ( $1043, 963, 603$  and  $574\text{ cm}^{-1}$ ), while the intensities of carbonate bonds, e.g.  $875\text{ cm}^{-1}$ , are

significantly increased. The F...OH peak at  $734\text{ cm}^{-1}$  shows higher intensity for CHA with respect to Si-Mg-FA. This, once again, confirms the CHA formation on Si-Mg-FA [27].

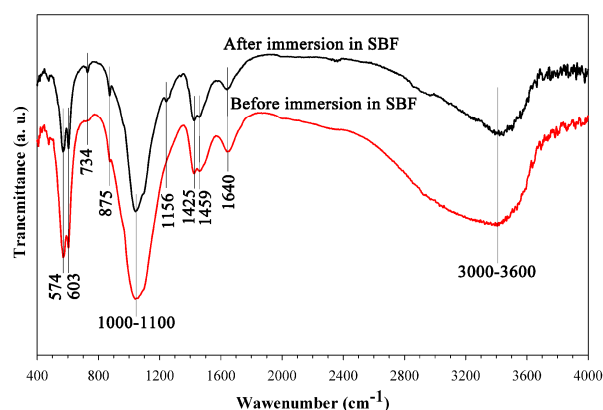


**Figure 4.** FTIR spectra of Si-Mg-FA before and after being soaked in SBF.

### 3.3. In vitro cell behavior

Table 2. shows MTT assay results after 24, 72 and 168 h incubation. There is a small statistical difference between control and Si-Mg-FA after 24 h ( $P < 0.05$ ), while a significant difference is observed between FA and Si-Mg-FA at this time ( $P < 0.05$ ). It has been reported that with increasing the  $\text{Ca}^{2+}$  concentration, number of living cells is increased in the cell culture medium [28]. FA decreases the  $\text{Ca}^{2+}$  release in the culture medium due to its low solubility and thereby cell proliferation is inhibited.

**TABLE 2.** MTT test results of control, FA and Si-Mg-FA at 540 nm after 24, 72 and 168 h cell culture.

sample	Number of samples	Colorimetric reading average OD( SD)
Control 24h	3	$0.7477 \pm 0.1186$
FA 24h	3	$0.2947 \pm 0.01097$
Si-Mg-FA 24h	3	$1.232 \pm 0.09784$
Control 72h	3	$2.576 \pm 0.3455$
FA 72h	3	$0.2283 \pm 0.02974$
Si-Mg-FA 72h	3	$2.228 \pm 0.1727$
Control 168h	3	$2.111 \pm 0.1254$
FA 168h	3	$0.11913 \pm 0.001528$
Si-Mg-FA 168h	3	$1.453 \pm 0.2530$

Former research showed that calcium and silicate ions of bioactive glass stimulate cell proliferation and gene expression [29]. After 72 h, the absorbance is significantly increased, indicating that the number of living cells is increased, i.e. the cells are proliferated. At this time, there is no significant difference between control and Si-Mg-FA ( $P < 0.05$ ). Fibroblasts have high proliferation rates and there is not enough space for

them; hence, the cell viability is decreased after 168 h. (Figure 5.)

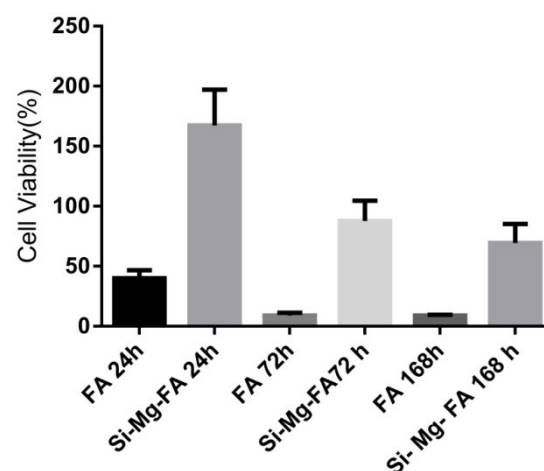


**Figure 5.** Dielectric constant ( $\epsilon$ ) mixtures activated for different times and sintered at  $1390^\circ\text{C}$  in microwave (MWS) and Conventional furnace (CS).

These results combined with invert microscopic images (Figure 6.) verify that Si-Mg-FA has less cytotoxicity. The SEM images of cell attachment are shown in Figure 7. It is evident that a good cell attachment is occurred and the cells are spread well, especially for FA samples. As illustrated in Figure 7. FA disks provide better cell attachment than Si-Mg-FA ones. FA produces a low surface potential which favors cell attachment [28].

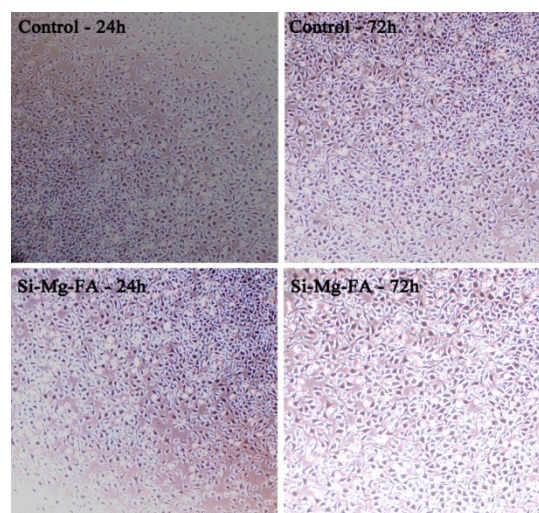


**Figure 6.** Invert microscopic images of media containing Si-Mg-FA and control after 24 and 72 h of cell culture.

It should be emphasized that presence of Si in FA enhances bioactivity and cell proliferation because it increases dissolution rate of apatites. This behavior can be explained by two mechanisms. It is known that dissolution begins at various defects including dislocations, grain boundaries and triple junctions which are introduced into the crystal lattice by incorporating Si

in apatite [30]. Substituting silicate ions into the apatite lattice distort and destabilize the structure, thereby increasing the dissolution to obtain energetically stabilize structure [31]. In addition, the Si-Mg-FA compound was synthesized by high energy ball milling during which various defects and internal strain are introduced into the lattice; thus, dissolution of apatite is increased leading to the enhanced bioactivity and cell proliferation. Finally, it is concluded that Si-Mg-FA has no cytotoxicity and can be used as a bone substitution material due to its bioactivity and biocompatibility.

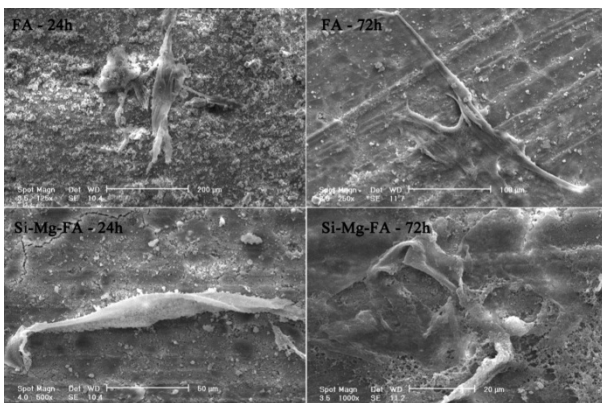


**Figure 7.** SEM images showing morphology of the cells cultured for 24 and 72 h on the surfaces of the FA and Si-Mg-FA disks showing the differences in the response of the cells to the different materials.

#### 4. CONCLUSIONS

Mechanically activated nanosized Si-Mg-doped Fluorapatite which was prepared after 12 h ball milling showed better bioactivity and cell response in comparison to mechanically activated nanosized fluorapatite. With substituting the Si and Mg, the solubility of Si-Mg-FA nanopowders was increased in comparison to FA, so the adsorption of  $\text{Ca}^{2+}$  ions onto the powders surfaces was simultaneously increased. The amount of agglomerated bone-like apatite formed on Si-Mg-FA was more than FA. Formation of carbonate hydroxyapatite (bone-like apatite) on the surfaces of samples soaked in SBF was approved. MTT results revealed that Si-Mg-FA possesses improved cell proliferation and cell viability, while it seemed that FA has better cell attachment. It was concluded that Si and Mg doping improves the bioactivity and cell proliferation of FA.

#### 5. ACKNOWLEDGMENTS

The authors are grateful for support of this research by Isfahan University of Technology.

#### REFERENCES

1. Shuai, C., Li, P., Liu, J. and Peng, S., "Optimization of TCP/HAP ratio for better properties of calcium phosphate

- scaffold via selective laser sintering", *Materials Characterization*, Vol. 77, (2013), 23–31.
2. Sharifnabi, A., Eftekhari Yekta, B., Fathi, H.M., Hossainipour, M., "Synthesis and characterization of nanosized magnesium-doped fluorapatite powder and coating for biomedical application", *Sol-Gel Science and Technology*, Vol.74, (2015), 66–77.
3. Taddei, P., Tinti, A., Reggiani, M., Monti, P. and Fagnano, C. "In vivo bioactivity of titanium and fluorinated apatite coatings for orthopaedic implants: a vibrational study", *Journal of Molecular Structure*, Vol. 3, (2003), 427–431.
4. Best, S.M., Porter, A.E., Thian, E.S. and Huang, J. "Bioceramics: Past, present and for the future", *Journal of the European Ceramic Society*, Vol. 28, No. 7, (2008), 1319–1327.
5. RZ, L. "Apatites in Biological Systems", *Progress in Crystal Growth and Characterization of Materials*, Vol. 4, (1981), 1–45.
6. Jha L.J., Best, S.M., Knowles J.C., Rehman I., Santos, J.D., Bonfield, W., "Preparation and characterization of fluoride-substituted apatites", *Journal of materials science Materials in medicine*, Vol. 8, (1997), 185–191.
7. Cai, Y., Zhang, S., Zeng, X., Wang, Y., Qian, M. and Weng, W., "Improvement of bioactivity with magnesium and fluorine ions incorporated hydroxyapatite coatings via sol – gel deposition on Ti6Al4V alloys", *Thin Solid Films*, Vol. 517, No. 17, (2009), 5347–5351.
8. Sharifnabi, A., Fathi, M.H., Yekta, B.E. and Hossainipour, M. "The Structural and Bio-corrosion Barrier Performance of Mg-substituted Fluorapatite Coating on 316L Stainless Steel Human Body Implant", *Applied Surface Science*, Vol. 288, (2014), 331-340.
9. Zahrani, E.M., Fathi, M.H. and Alfantazi, A.M. "Sol-Gel Derived Nanocrystalline Fluoridated Hydroxyapatite Powders and Nanostructured Coatings for Tissue Engineering Applications", *Metallurgical and Materials Transaction A*, Vol. 24A, (2011), 3291-3309.
10. Pullen, L.J. and Gross, K.A., "Dissolution and mineralization of sintered and thermally sprayed hydroxy-fluoroapatites", *Journal of materials science. Materials in medicine*, Vol. 16, No. 5, (2005), 399–404.
11. Chien, C.S., Liao, T.Y., Hong, T.F., Kuo, T.Y., Wu, J.L. and Lee, T.M., "Investigation into microstructural properties of fluorapatite Nd-YAG laser clad coatings with PVA and WG binders", *Surface and Coatings Technology*, Vol. 205, No. 10, (2011), 3141–3146.
12. Fathi, M.H., Zahrani, E.M. and Zomorodian, A., "Novel fluorapatite/niobium composite coating for metallic human body implants", *Materials Letters*, Vol. 63, No. 13–14, (2009) 1195–1198.
13. Cheng, K., Shen, G., Weng, W. and Han, G., "Synthesis of hydroxyapatite/fluoroapatite solid solution by a sol – gel method", *Materials Letters*, Vol. 51, (2001), 37–41.
14. Porter, A.E., Patel, N., Skepper, J.N., Best, S.M. and Bonfield, W., "Comparison of in vivo dissolution processes in hydroxyapatite and silicon-substituted hydroxyapatite bioceramics", *Biomaterials*, Vol. 24, (2003), 4609–4620.
15. Hijón, N., Victoria Cabañas, M., Peña, J. and Vallet-Regí, M., "Dip coated silicon-substituted hydroxyapatite films", *Acta biomaterialia*, Vol. 2, No. 5, (2006), 567–574.
16. Hench, L.L., *Sol-Gel Silica Properties, Processing and Technology Transfer, chapter 10, biological Implication*. (1993), 116–163.
17. Fathi, M.H. and Mohammadi Zahrani, E., "Mechanical alloying synthesis and bioactivity evaluation of nanocrystalline fluoridated hydroxyapatite", *Journal of Crystal Growth*, Vol. 311, No. 5, (2009), 1392–1403.

18. Koch, C.C. "Mechanical Milling and Alloying", *Material Science and Technology A*, Vol. 15, (1991), 193–245.
19. Ahmadi, T., Monshi, A., Mortazavi, V., Fathi, M.H., Sharifi, S., HashemiBeni, B., Moghare Abed, A., Kheradmandfard, M. and Sharifnabi, A., "Synthesis and dissolution behavior of nanosized silicon and magnesium co-doped fluorapatite obtained by high energy ball milling", *Ceramics International*, Vol. 40, (2014), 8341–8349.
20. Kokubo, T. and Takadama, H. "How useful is SBF in predicting in vivo bone bioactivity?", *Biomaterials*, Vol. 27, (2006), 2907–2915.
21. Kiany, M. and Ebadzadeh, T., "Effect of mechanical activation and microwave sintering on crystallization and mechanical strength of cordierite nanograins", *Ceramic International*, Vol. 41, No. 2, (2015), 2342–2347.
22. Bohner, M. and Lemaitre, J., "Can bioactivity be tested in vitro with SBF solution?", *Biomaterials*, Vol. 30, (2009), 2175–2179.
23. Kim, H.M., Himeno, T., Kokubo, T. and Nakamura, T., "Process and kinetics of bonelike apatite formation on sintered hydroxyapatite in a simulated body fluid", *Biomaterials*, Vol. 26, (2005), 4366–4373.
24. Duan, Y.R., Zhang, Z.R., Wang, C.Y., Chen, J.Y. and Zhang, X.D., "Dynamic study of calcium phosphate formation on porous HA / TCP ceramics", *Biomaterials*, Vol. 6, (2005), 795–801.
25. Gu, Y.W., Khor, K.A. and Cheang, P., "Bone-like apatite layer formation on hydroxyapatite prepared by spark plasma sintering (SPS)", *Biomaterials*, Vol. 25, (2004), 4127–4134.
26. Zhang, Q., Chen, J., Feng, J., Cao Y. and Deng, C. "Dissolution and mineralization behaviors of HA coatings", *Chemical Engineering*, Vol. 24, (2003), 4741–4748.
27. Kheradmandfard, M., Fathi, M.H., Ahangarian, M.E. and Zahrani, M., "In vitro bioactivity evaluation of magnesium-substituted fluorapatite nanopowders", *Ceramics International*, Vol. 38, (2012), 169–175.
28. Cheng, K., Weng, W., Wang, H., Zhang, S. "In vitro behavior of osteoblast-like cells on fluoridated hydroxyapatite coatings", *Biomaterials*, Vol. 26, (2005), 6288–6295.
29. Zhao, W., Wang, J., Zhai, W., Wang, Z. and Chang, J., "The self-setting properties and in vitro bioactivity of tricalcium silicate", *Biomaterials*, Vol. 26, (2005), 6113–6121.
30. Porter, A.E., Patel, N., Skepper, J.N., Best, W. and Bonfield, S.M., "Comparison of in vivo dissolution processes in hydroxyapatite and silicon-substituted hydroxyapatite bioceramics", *Biomaterials*, Vol. 24, (2003), 4609–4620.
31. Botelho, C.M., Lopes, M.A., Gibson, I.R., Best, S.M. and Santos, J.D., "Structural analysis of Si-substituted hydroxyapatite: zeta potential and X-ray photoelectron spectroscopy", *Journal of Materials Science. Materials in Medicine*, Vol. 13, (2002), 1123–1127.